Osteoarthritis and Cartilage Open 5 (2023) 100389

Contents lists available at ScienceDirect

Osteoarthritis and Cartilage Open

journal homepage: www.elsevier.com/journals/osteoarthritis-and-cartilage-open/2665-9131

Development of a novel animal model of rotator cuff tear arthropathy replicating clinical features of progressive osteoarthritis with subchondral bone collapse

T. Ijuin [a,b], T. Iuchi [a], H. Tawaratsumida [a], Y. Masuda [a,c], A. Tokushige [d], S. Maeda [e,*], N. Taniguchi [a,b,c,e]

[a] Department of Orthopaedic Surgery, Graduate School of Medical and Dental Sciences, Kagoshima University, Kagoshima, Kagoshima 890-8520, Japan
[b] Department of Medical Joint Materials, Graduate School of Medical and Dental Sciences, Kagoshima University, Kagoshima, Kagoshima 890-8520, Japan
[c] Department of Locomotory Organ Regeneration, Graduate School of Medical and Dental Sciences, Kagoshima University, Kagoshima, Kagoshima 890-8520, Japan
[d] Department of Clinical Pharmacology and Therapeutics, Graduate School of Medicine, University of the Ryukyus, Nakagami Gun Nishihara Cho, Okinawa 903-0213, Japan
[e] Department of Bone and Joint Medicine, Graduate School of Medical and Dental Sciences, Kagoshima University, Kagoshima, Kagoshima 890-8520, Japan

ARTICLE INFO

Keywords:
Cuff tear arthropathy
Osteoarthritis
Subchondral bone collapse
Long head of biceps
Capsuloligamentous complex
Fibrous cells

ABSTRACT

Objective: To establish an animal model of modified cuff tear arthropathy (mCTA) in order to better replicate the pathophysiology associated with rotator cuff tear-induced humeral head collapse.
Design: mCTA was induced by transection of the rotator cuff, the long head of the biceps brachii (LHB), and superior half of the joint capsule in the right shoulder of 12-week-old rats; the left shoulder underwent sham surgery. The severity of CTA was quantitated using the Murine Shoulder Arthritis Score (MSAS). The trabecular bone of the humeral head and metaphysis was analyzed using bone histomorphometry. The expression of proinflammatory cytokines and catabolic enzymes was evaluated immunohistochemically.
Results: In the mCTA model, the MSAS increased starting from 2 weeks after induction, and there was notable subchondral bone collapse with fibrous cells at 4 weeks. The mCTA cartilage exhibited positive staining for TNF-α, IL-1β/6, MMP-3/13, and ADAMTS5. The trabecular bone volume was reduced not only in the subchondral bone but also in the metaphysis of the humeri, and bone resorption was enhanced in these areas. In the collapsed subchondral bone, both bone formation and resorption were increased. The fibrous cells showed expression of TNF-α, IL-6, and MMP-13, along with specific markers of mesenchymal stem cells. Furthermore, the fibrous cells showed osteoblastic characteristics (RUNX2-positive) and expressed RANKL.
Conclusions: The LHB and the capsuloligamentous complex are critical stabilizers of the glenohumeral joint, serving to prevent the advancement of CTA following massive rotator cuff tears. Fibrous cells appear to play a role in the humeral head bone resorption.

1. Introduction

The shoulder joint is the most mobile joint in the human body [1]. The static stabilizers are the glenoid labrum and the capsuloligamentous complex (superior capsule), and the dynamic stabilizers are the long head of biceps brachii (LHB) and the rotator cuff [2,3]. Following massive tears of the rotator cuff, the combination of severe pain and coupled muscle force defects results in severe deformity of the glenohumeral joint; cuff tear arthropathy (CTA) [4]. CTA is characterized by key radiographic features such as collapse in the proximal region of the humeral articular surface without the large osteophytes that are characteristic of osteoarthritis (OA) [4–6]. The affected humerus is usually rounded off; this sign is called femoralization [4,7]. Histologically, the atrophic articular cartilage of the humeral head becomes infiltrated by fibroblastic cells, called fibrous pannus, that can be distinguished from the inflammatory pannus observed in rheumatoid arthritis (RA) [4]. The trabecular bone volume of the humeral head is decreased, and this is accompanied by collapse of the subchondral bone in the superior part;

* Corresponding author. Department of Bone and Joint Medicine, Graduate School of Medical and Dental Sciences, Kagoshima University, 8-35-1 Sakuragaoka, Kagoshima 890-8520, Japan.
E-mail address: s-maeda@m3.kufm.kagoshima-u.ac.jp (S. Maeda).

https://doi.org/10.1016/j.ocarto.2023.100389
Received 18 July 2023; Accepted 21 July 2023

the term CTA is used only when there is the presence of subchondral bone collapse in the humeral head [4].

The rat was found to have the only shoulder structure among the evaluated 33 species of laboratory-use animals [8] that resembled that of the humans, particularly in the subacromial region and in terms of the anatomic relationship between the supraspinatus (SSP) tendon and the acromion, coracoid, clavicle, and SSP fossa. Accordingly, Kramer et al. [9] established two separate CTA models by transection of the SSP and ISP tendons (tenotomy) or the suprascapular nerve (denervation) in 3-month-old rats. After 12 weeks, they found that the cartilage of the humeral head was degenerated to a similar extent in both the tenotomy and denervation models. This finding suggests that the loss of nutrient factors in the joint fluid by rotator cuff tears is not the main cause of CTA, but rather altered biomechanical loading in the glenohumeral joint surface plays a pivotal role [9]. Zingman et al. [10] created a rotator cuff transection model by detaching not only the SSP and ISP tendons but also the tendon of the teres minor muscle in 3-month-old mice. In this mouse model, features of OA in the humeral head were observed from 14 weeks and were accelerated up to 45 weeks after surgery [10]. However, there are aspects that do not fully reflect the actual clinical findings of CTA. Firstly, the onsets of CTA phenotype are delayed compared to actual clinical practice. It has been reported that CTA changes in humans can occur within 5 years following rotator cuff tears [11,12]. Given that 10.5 rat days or 8.82 mice days are equivalent to 1 human year during mature adulthood [13,14], these postoperative observation periods of 12 weeks in rats or 45 weeks in mice account for approximately 8 or 36 years of human life, respectively. Secondly, it is rare for the teres minor tendon to tear in human cases [15], making it a problematic aspect of the mouse model. Thirdly, these models lack the crucial CTA feature of subchondral bone collapse and bone loss of the humeral head. Finally, in the existing CTA models, neither the superior capsule nor the LHB tendon is included in the procedure.

The indispensable role of the capsuloligamentous complex is well described in regard to shoulder stability [16,17]. It is composed of two ligament limbs, and both of which are connected by a transverse ligamentous structure called the rotator cable [18]. It provides a hammock-like structure that prevents direct impact of the humeral head and the acromion [3], and creates a suspension bridge phenomenon that allows a patient with a partially torn rotator cuff to maintain shoulder function [3]. Patients with irreparable rotator cuff tears have a defect of the superior capsule [19]. Meanwhile, the LHB tendon is important for the stability of the glenohumeral joint [20,21], and detaching the LHB tendon in cases of rotator cuff tears (for pain control) can lead to the appearance or exacerbation of CTA [22]. Moreover, severe CTA is often accompanied by the rupture of the LHB tendon at a high rate [23]. Therefore, combined destruction of the superior capsule and the LHB tendon is likely to be the crucial event allowing CTA to progress. Since this concept has not been investigated in animal models, the objective of this study was to develop a modified CTA rat model.

2. Method

2.1. Rotator cuff tenotomy (RCT) and modified CTA (mCTA) models

All animal experiments were approved by the Institutional Animal Care and Use Committee of Kagoshima University (# MD21024, #MD22038) and carried out according to the Kagoshima University Animal Experimentation Regulations. 12-week-old male Sprague–Dawley rats were used (n = 7 each for respective time point).

The sole RCT model was generated as previously reported [9]. Briefly, in the right shoulder of rats, a longitudinal incision was made through the deltoid, and the SSP and ISP tendons were cut at their insertion into the humeral head. The biceps and capsule were left intact. Sham incisions of the skin and deltoid were made in the left shoulder.

To generate the rat mCTA model, in the right shoulder, the deltoid muscle was incised in a T-shape, and the SSP and ISP tendons were resected at their insertion into the humeral head. The superior half of the capsule and the LHB tendon were then resected. The left shoulder joint underwent sham surgery involving skin and deltoid incisions. Plain X-ray imaging of both rat shoulder joints was performed at radiation of 40 kV/4.0 mAs using the mobile X-ray equipment IME-100A (Toshiba Medical Manufacturing, Otawara, Japan).

2.2. Histology and immunohistochemistry (IHC)

The humeral articular cartilage was divided into three regions (superior, middle, and inferior), as previously reported [9]. Safranin O staining was employed to measure the thickness of the articular cartilage at 20 locations in each region, and the average was calculated as previously reported [10]. Alcian blue (pH 1.0) staining was performed for assessment of the OA change using the Murine Shoulder Arthritis Score (MSAS) [10]. Zingman et al. developed the MSAS because they found that the checkpoints of the several features of knee OA included in the existing Mankin and Osteoarthritis Research Society International arthritis scoring systems were not to be features of shoulder OA [10].

For the bone histomorphometric analysis, the rats were intraperitoneally injected with calcein (8 mg/kg) at 5 days and 1 day before sacrifice. Glycidyl methacrylate resin-embedded 3 μm-thick sections were stained with toluidine blue. The humeral metaphysis was analyzed at Kureha Special Laboratory using a Histometry RT Camera (System Supply Co., Nagano, Japan), and we analyzed the humeral head subchondral bone using BZ-X710/BZ-X700 microscope systems and BZ-X Analyzer software (Keyence Corporation, Osaka, Japan).

For IHC, sections were subjected to antigen retrieval, endogenous peroxidase inactivation, and blocking. The primary antibodies used in this study are described in the Supplementary Information. Normal rabbit or mouse IgG served as a negative control. Histofine Simple Stain Rat MAX PO (MULTI) (Nichirei Biosciences, Tokyo, Japan) was applied as a secondary antibody. Signals were visualized using diaminobenzidine solution. Counterstaining was performed with Mayer's hematoxylin solution. Images were captured using the BZ-X710/BZ-X700 microscope system. For quantification of the positive staining rate, the number of signal-positive cells was divided by the total cell number.

2.3. Statistical analysis

SAS software JMP version 16.0 (SAS Institute, Cary, NC, USA) was used for the statistical analysis. The results are expressed as mean ± 95% confidence intervals. Normality was assessed using the Shapiro-Wilk test; all the results were non-parametric. The Wilcoxon rank sum test was performed to compare the mean between the two groups according to its distribution. The Kruskal-Wallis test followed by the Steel-Dwass test was used for between-group comparisons. Statistical significance was defined as $p < 0.05$.

More detailed methods are provided in the Supplemental Information.

3. Results

3.1. RCT in adult rats induces only limited degeneration of humeral head articular cartilage in 4 weeks

First, we verified the effect of sole RCT on humeral head articular cartilage degeneration in adult rats. We found that the transected tendons of the SSP and ISP muscles were reconnected by granulation tissue infiltrated with inflammatory cells as early as 1 week after surgery, and they were further reconstructed by scar tissue within 4 weeks (Fig. 1A). The humeral head cartilage of the RCT-treated shoulder did not show any apparent changes after one week, but showed a slight decrease in Alcian blue staining intensity in the superior region, marginally increasing the MSAS at 4 weeks, while the cartilage in the middle and inferior regions was unaffected (Fig. 1B and C).

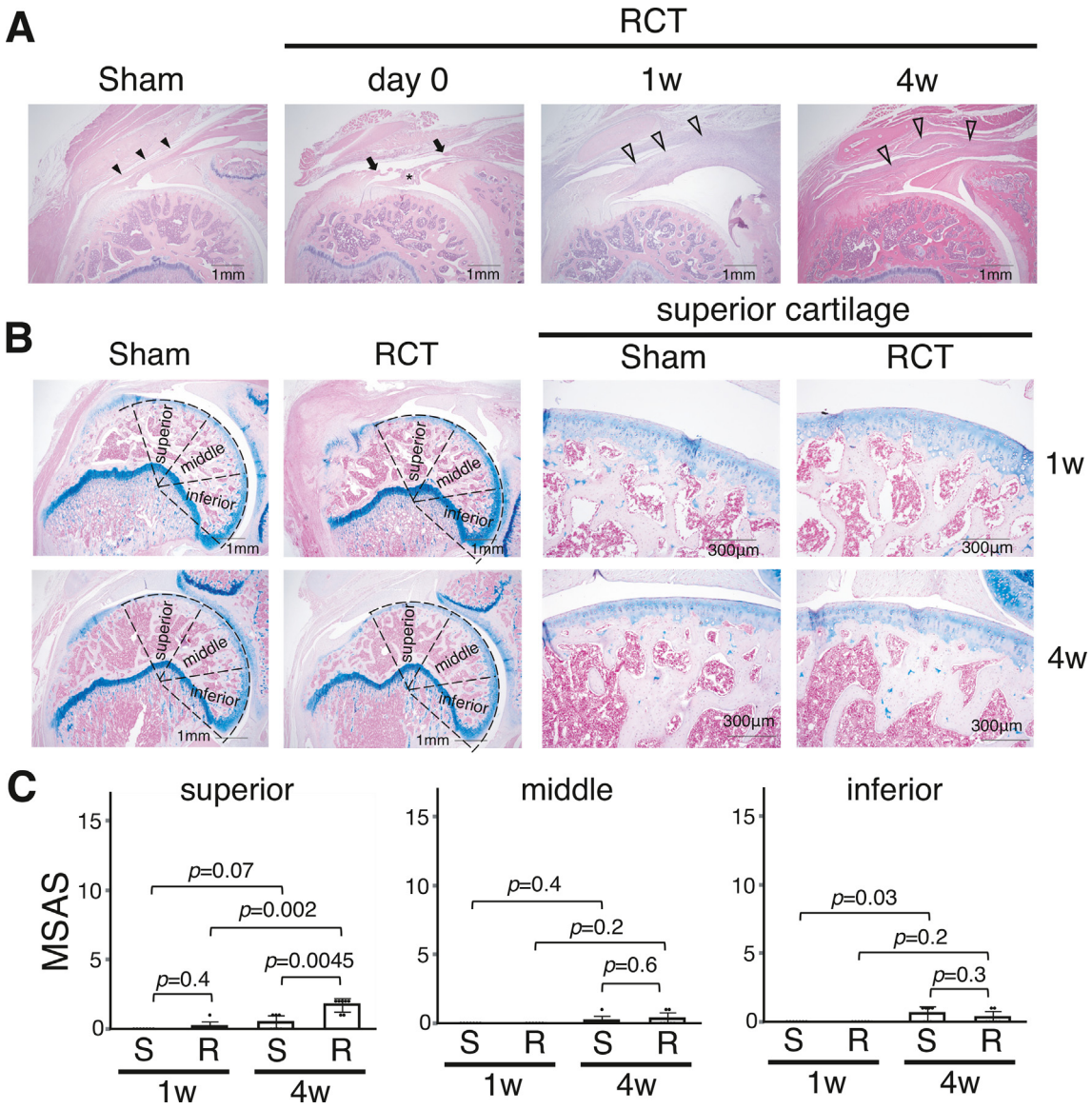

Fig. 1. RCT in adult rats induced only limited arthropathy in 4 weeks. (A) RCT alone was applied by transecting the tendons of the supraspinatus and infraspinatus muscles in adult rats. The arrowheads denote the intact rotator cuff tendons in the sham shoulder. The asterisk (day 0) denotes the intact capsule in the RCT shoulder. The transected tendons (arrows denote the stumps at day 0) were reconnected by granulation tissue infiltrated with inflammatory cells (open arrowheads at 1w), which was replaced by scar tissue at 4w (open arrowheads). (B) Alcian blue staining was performed to evaluate the MSAS at 1 and 4w. The left panels illustrate the superior, middle, and inferior cartilage areas. The right panels show the magnified images of the superior cartilage regions. (C) The severity of the arthropathy was evaluated by the MSAS (n = 7). S = Sham; R = RCT. The Wilcoxon rank-sum test was used. RCT, rotator cuff tenotomy; MSAS, Murine Shoulder Arthritis Score; w, weeks.

3.2. Combined transection of LHB, superior half of shoulder joint capsule and rotator cuff tendons in adult rats leads to rapidly progressive arthropathy

To induce irreversible instability of the glenohumeral joint in adult rats, we transected the SSP and ISP tendons, the LHB, and the superior part of the capsuloligamentous complex (Fig. 2A–D); we designated this model as modified CTA (mCTA). As a result, the humeral head could be easily dislocated by pulling out the SSP stump (Fig. 2D). The stumps of the rotator cuff tendon and the capsule were histologically confirmed at day 0 (Fig. 2E).

Four weeks after the mCTA induction, gross inspection of the humeral head revealed drastic changes: the color tone of the articular cartilage surface showed a decrease in redness, and the rough texture became noticeable, especially in the superior region (Fig. 3A). The cartilage depth was measured in the superior, middle, and inferior areas of the humeral head (Fig. 3B and C); it was found to be exclusively reduced in the superior region in a time-dependent manner during the 8-week observation period, except in the middle area in which the cartilage was mildly thicker in the mCTA-affected humeri at 8 weeks (Fig. 3C). In the mCTA-affected shoulders, deteriorations were observed in the sphericity of the articular portion of the humeral head, chondrocyte cellularity, subchondral bone morphology, and dyeability of Alcian blue, while fibrous cells emerged and covered the destroyed subchondral bone from 4 weeks (Fig. 3D and E). However, similar to the result of sole RCT (Fig. 1), the resected rotator cuff tendon was reconnected by scar tissue within 2 weeks (Fig. 3D). Importantly, collapse of the subchondral bone was evident from 4 weeks after mCTA induction (Fig. 3D). The time-dependent arthritic alterations were prominent in the superior region, milder deformities were observed in the middle part, and the inferior area remained intact (Fig. 3E). However, no evident signs of arthritic changes were detected in the evaluation through plain X-rays at 4 weeks after mCTA induction.

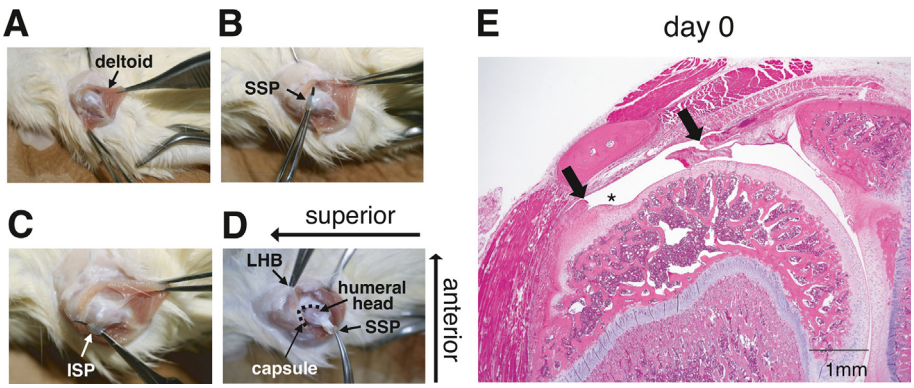

Fig. 2. Generation of modified cuff tear arthropathy model in adult rats. In the right shoulder of adult rats, (A) the deltoid muscle was split and (B) the SSP and (C) ISP tendons were resected at their insertion into the humeral head. (D) The superior half of the capsule was then resected (broken line), and the LHB was transected. The left shoulder joint underwent sham surgery involving only a deltoid incision. (E) Histology of hematoxylin-eosin staining at day 0 shows the stumps of the transected tendons (arrows) and the superior capsule (asterisk). SSP, supraspinatus; ISP, infraspinatus; LHB, long head tendon of the biceps brachii.

3.3. Increased expression of OA-related proinflammatory cytokines and catabolic enzymes in mCTA-affected cartilage and synovium

We evaluated the expression of OA-associated proteins by IHC and found that TNF-α, IL-1β, IL-6, MMP-3, MMP-13, and ADAMTS-5 were increased in and around approximately 70%–80% of the chondrocytes in the superior part of the articular cartilage of the mCTA humeral head. This increase persisted from 2 weeks and remained unchanged until 8 weeks. (Fig. 4). In the synovium adjacent to the humeral head, expression of TNF-α and IL-1β was observed in more than 50% of cells from 2 weeks after mCTA induction. The expression gradually increased to approximately 80% at 8 and 4 weeks, respectively. IL-6 exhibited a weak increase in expression starting from 4 weeks, while MMP-3 showed a modest increase starting from 2 weeks. No evident increase in expression was observed for MMP-13. ADAMTS-5 exhibited a gradual increase in expression from 2 to 8 weeks, reaching a level of approximately 20% (Fig. 5).

3.4. Attenuation of bone volume in mCTA-affected humeral head

We conducted a bone histomorphometric evaluation of the subchondral and metaphyseal bone in the humeral head (Fig. 6A). The bone volume of the subchondral bone significantly decreased from 4 weeks after mCTA induction (Fig. 6B). The number of osteoclasts, a bone resorption parameter, increased from 2 weeks and remained at that level until 8 weeks (Fig. 6C). There were no obvious changes in the bone formation parameters of mineral apposition rate and bone formation rate at 4 weeks (Fig. 6D). In the metaphyseal bone, we unexpectedly found reductions in volume starting from 2 weeks after mCTA induction (Fig. 6E). The thickness and the number of the trabecular bone were decreased at 4 weeks (Fig. 6F). The number of osteoclasts was increased from 2 weeks (Fig. 6G), and the osteoclast surface and the bone surface erosion were increased at 4 weeks (Fig. 6H); by contrast, the surface of osteoblasts, mineral apposition rate, and bone formation rate remained unchanged in the mCTA-affected metaphysis (Fig. 6I).

3.5. High bone turnover in collapsed subchondral bone of mCTA-affected humeral head

We further analyzed the histomorphometry of the collapsed subchondral bone in the mCTA model. Calcein double labeling revealed the increased rates of mineral apposition and bone formation (Fig. 7A), while the IHC for cathepsin K showed increased multi-nucleated osteoclasts in this region (Fig. 7B), indicating high bone turnover in the collapsed subchondral bone.

3.6. Protein expression profile of fibrous cells in mCTA

Finally, we immunohistochemically characterized the fibrous cells around the subchondral bone collapse site. The fibrous cells were present within the articular cartilage, gaps in the destructed subchondral bone, and the immediate adjacent bone marrow (Fig. 8A). These cells expressed TNF-α, IL-6, and MMP-13 (Fig. 8B), and mesenchymal stem cell (MSC)-specific markers CD34 and vimentin, but not CD68, a marker for RA pannus (Fig. 8C). Moreover, these fibrous cells were positive for other MSC-specific markers, leptin receptor [24] and PDGFRα [25] (Fig. 8C). We found that the fibrous cells expressed RUNX2, the master regulator of osteoblast differentiation [26], and were positive for RANKL (Fig. 8D).

4. Discussion

In this study, RCT alone in adult rats resulted in reconnection of the transected rotator cuff tendons by scar tissue within 1 week and only mild OA change in the humeral head after 4 weeks (Fig. 1). Additional transection of the LHB and the superior capsule (Fig. 2) induced severe humeral head OA with subchondral bone collapse within 4 weeks despite the reconnection of the rotator cuff (Fig. 3). Our results suggest that the LHB and the superior capsuloligamentous complex are the critical stabilizers of the glenohumeral joint that prevent arthropathy progression after massive rotator cuff tears. It is thus reasonable that the previously reported murine models of CTA induced by sole RCT or denervation showed mild humeral head OA but lacked the crucial CTA feature of subchondral bone collapse [9,10,27]. Importantly, however, there is no published paper evaluating the association between the extent of damage to the LHB and the joint capsule and the arthropathy Hamada grading [6] in CTA cases. Thus, our mCTA model provides important information regarding the pivotal role of the glenohumeral joint stabilizers that prevent CTA progression after rotator cuff tears.

Histologically, the CTA-affected humeral head lacks osteophytes and exhibits subchondral bone collapse [4]; additionally, the cartilage layer is thickened in the middle area, although the cartilage degenerative changes observed in the superior area are similar to those of OA [28]. Our rat mCTA model showed thinned cartilage in the superior part of the humeral head, whereas the cartilage in the middle part was mildly thickened after 8 weeks of induction (Fig. 3C), resembling human CTA. TNF-α, IL-1β, and IL-6 have been suggested to be the main proinflammatory cytokines involved in the pathophysiology of OA. These cytokines inhibit synthesis of type II collagen [29,30], the main collagen component in cartilage, and induce expression of cartilage catabolic enzymes: collagenases such as MMP-3 and MMP-13 [31,32] or ADAMTS-5 [33]. Notably, the expression of OA-related proinflammatory cytokines and catabolic enzymes had not been previously evaluated in either CTA specimens or primary shoulder OA samples. We demonstrated appreciable expression of TNF-α, IL-1β, IL-6, MMP-3, MMP-13, and ADAMTS-5 in rat mCTA cartilage (Fig. 4), suggesting that the pathophysiology of the cartilage degeneration itself resembles that of OA. It is accepted that synovial inflammation is a feature of human OA, and proinflammatory cytokines, MMPs, and ADAMTSs are commonly detected in the synovium [34,35]. We detected a relatively strong expression of TNF-α and IL-1β, as well as a mild expression of ADAMTS-5, in the

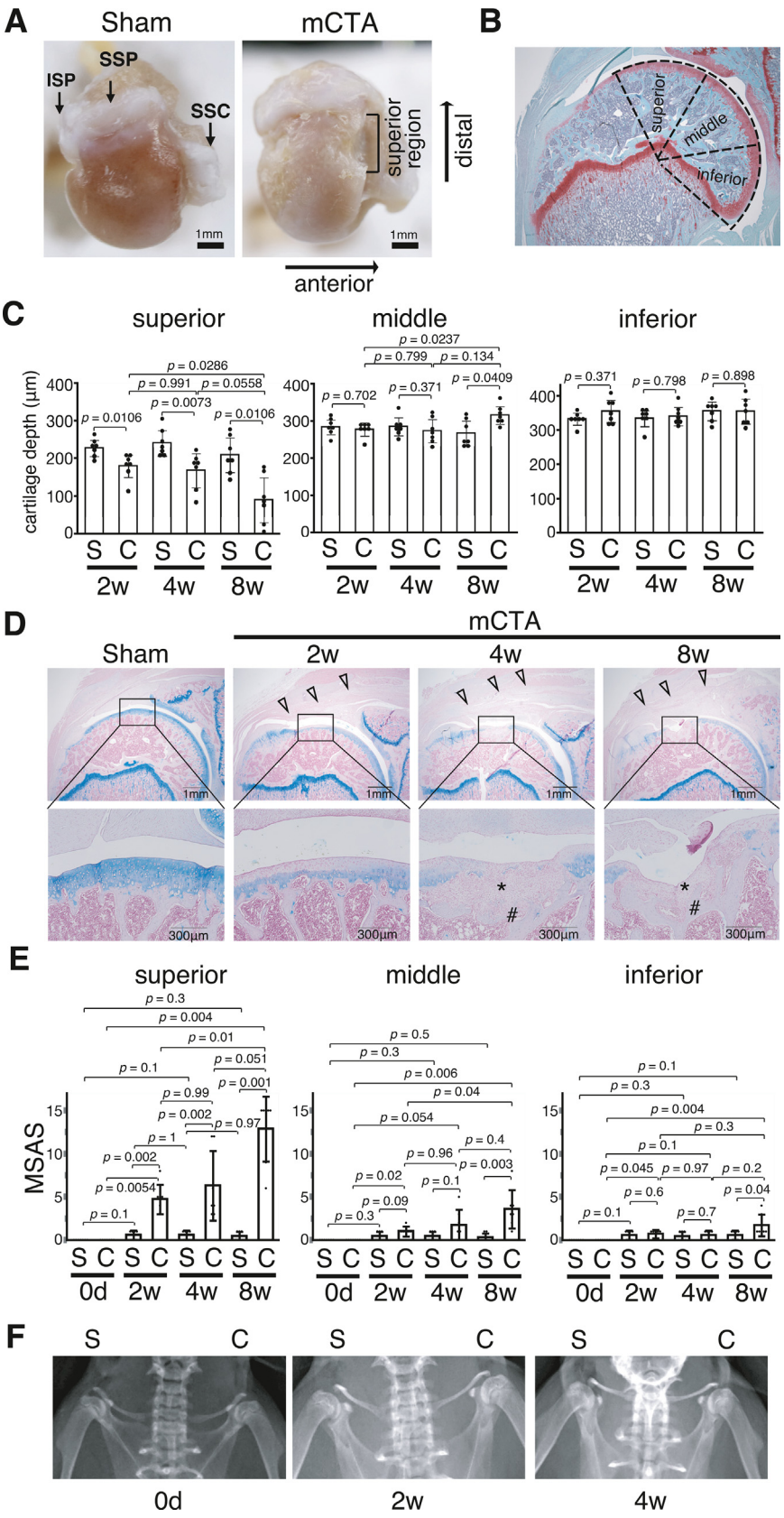

Fig. 3. Rapidly progressive arthropathy with subchondral bone collapse and fibrous cells in rat mCTA-affected humeral head. (A) Gross inspection of the humeral head 4 weeks after mCTA induction. (B, C) The depth of Safranin-O-stained cartilage was measured in the superior, middle, and inferior areas of the numeral head (n = 7). (D) Alcian blue staining was performed on the humeral head to evaluate the OA features after induction of mCTA by the MSAS at 2, 4, and 8 w. The transected rotator cuff tendons were reconnected by scar tissue (open arrowheads). The asterisk and cross-hatch indicate fibrous cells and collapsed subchondral bone, respectively. (E) The degree of OA changes was quantified using the MSAS (n = 7). (F) Plain X-ray images capturing both shoulders of rats at 0, 2, and 4 w. S = Sham; C = mCTA. Wilcoxon rank-sum test was performed for Sham vs. mCTA; Kruskal–Wallis and Steel–Dwass tests were performed for comparison between the groups at different time points. mCTA, modified cuff tear arthropathy; OA, osteoarthritis; MSAS, Murine Shoulder Arthritis Score; ISP, infraspinatus; SSP, supraspinatus; SSC, subscapularis; d, day; w, weeks.

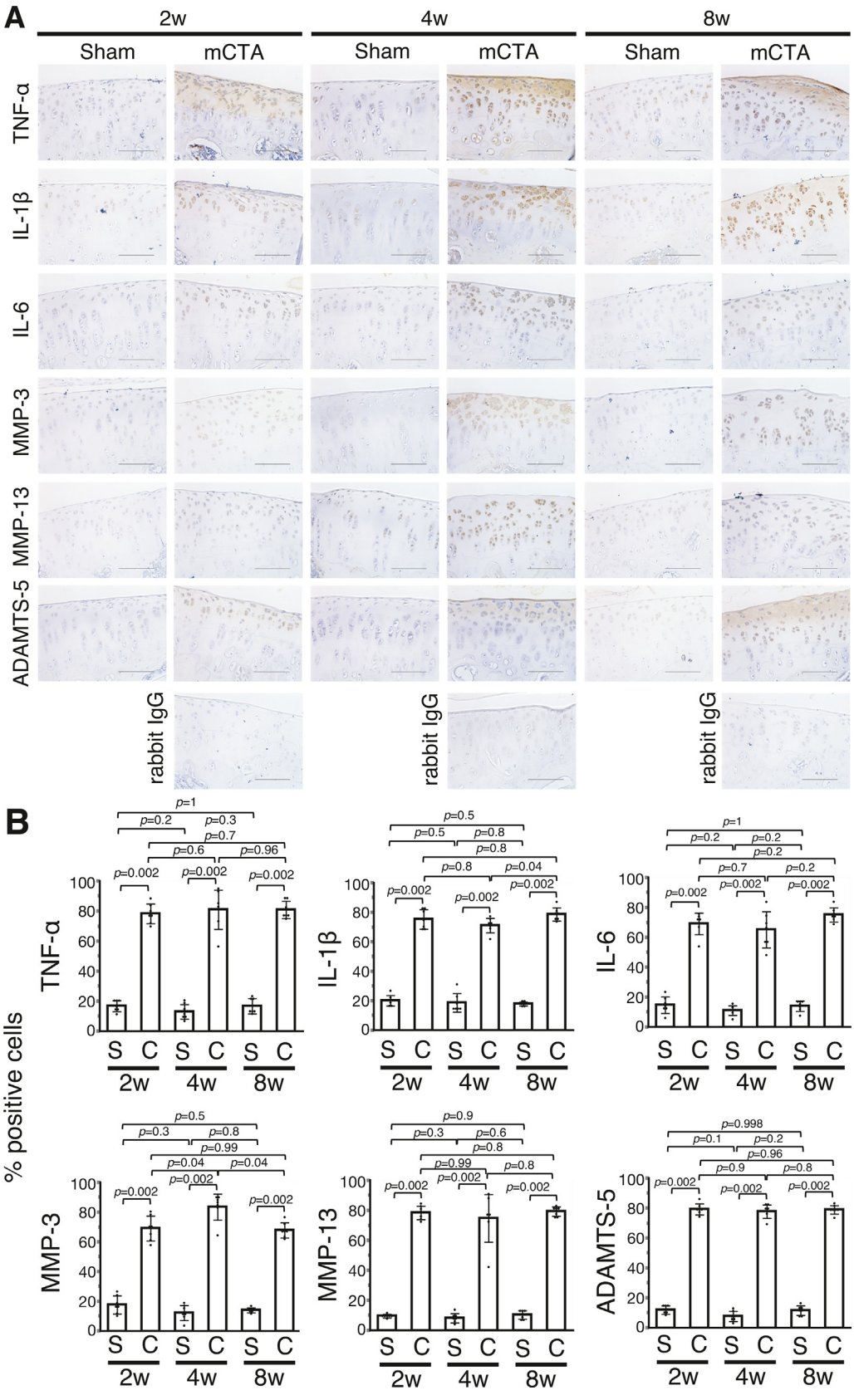

Fig. 4. Protein expression of osteoarthritis-related proinflammatory cytokines and catabolic enzymes in mCTA-affected cartilage. (A) Immunohistochemistry of the indicated proteins in the humeral head articular cartilage specimens was performed 2, 4, and 8 weeks after mCTA induction. Normal rabbit IgG served as a negative control for the primary antibodies. Images of the superior cartilage area are shown. Scale bar = 100 μm. (B) The number of positively stained chondrocytes was counted and expressed as the percent of the total number of articular chondrocytes (n = 7). S = Sham; C = mCTA. The Wilcoxon rank-sum test was performed. mCTA, modified cuff tear arthropathy; TNF, tumor necrosis factor; IL, interleukin; MMP, matrix metalloproteinase; ADAMTS, a disintegrin and metalloproteinase with thrombospondin motifs; IgG, immunoglobulin G.

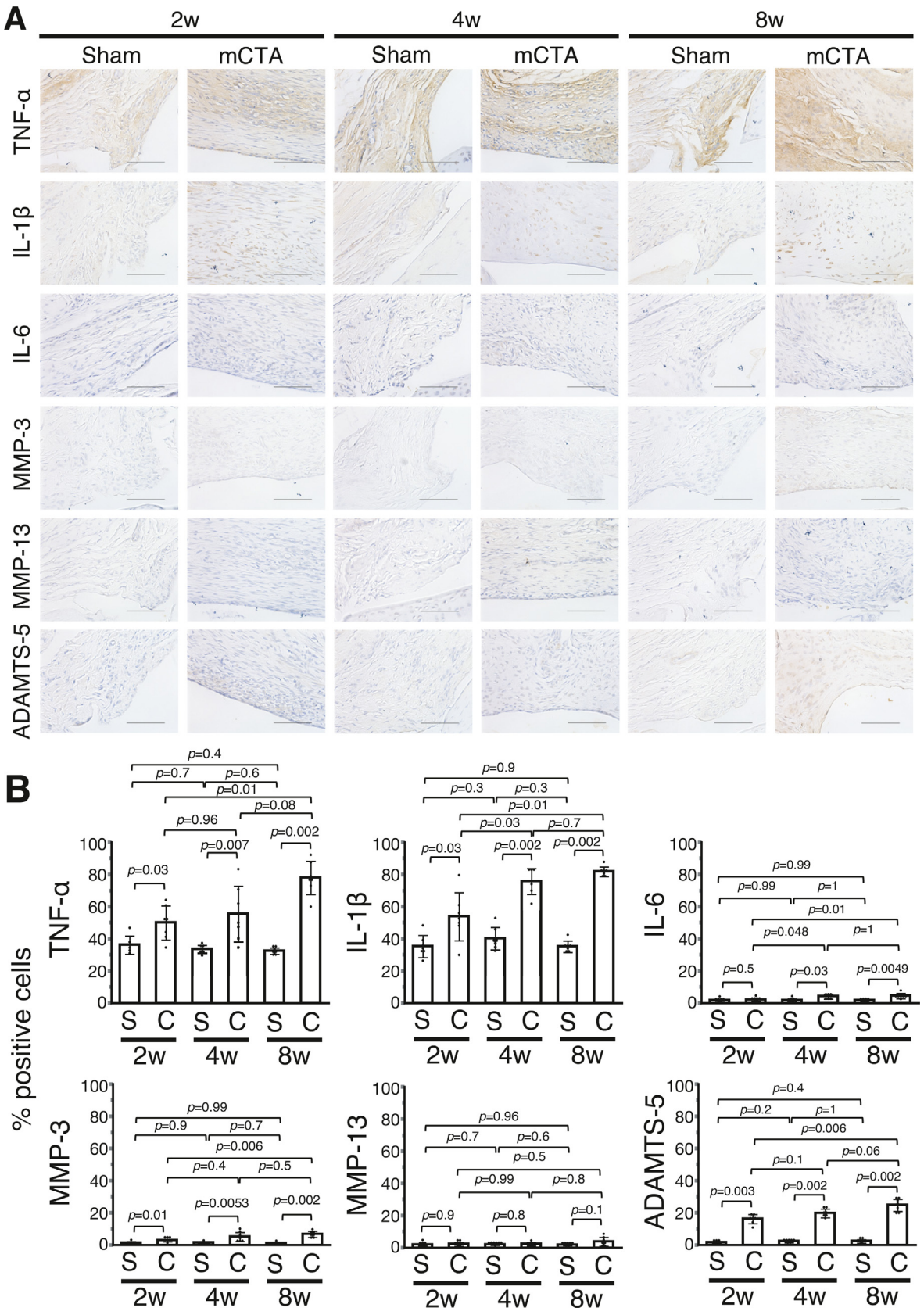

Fig. 5. Protein expression of osteoarthritis-related proinflammatory cytokines and catabolic enzymes in mCTA-affected synovium. (A) Immunohistochemistry of the indicated proteins in the synovium specimens was performed 2, 4, and 8 weeks after mCTA induction. Images of the synovium in close proximity to the resected rotator cuff are shown. Scale bar = 100 μm. (B) The number of positively stained cells was counted and expressed as the percent of the total cell number (n = 7). S = Sham; C = mCTA. The Wilcoxon rank-sum test was performed. mCTA, modified cuff tear arthropathy; TNF, tumor necrosis factor; IL, interleukin; MMP, matrix metalloproteinase; ADAMTS, a disintegrin and metalloproteinase with thrombospondin motifs.

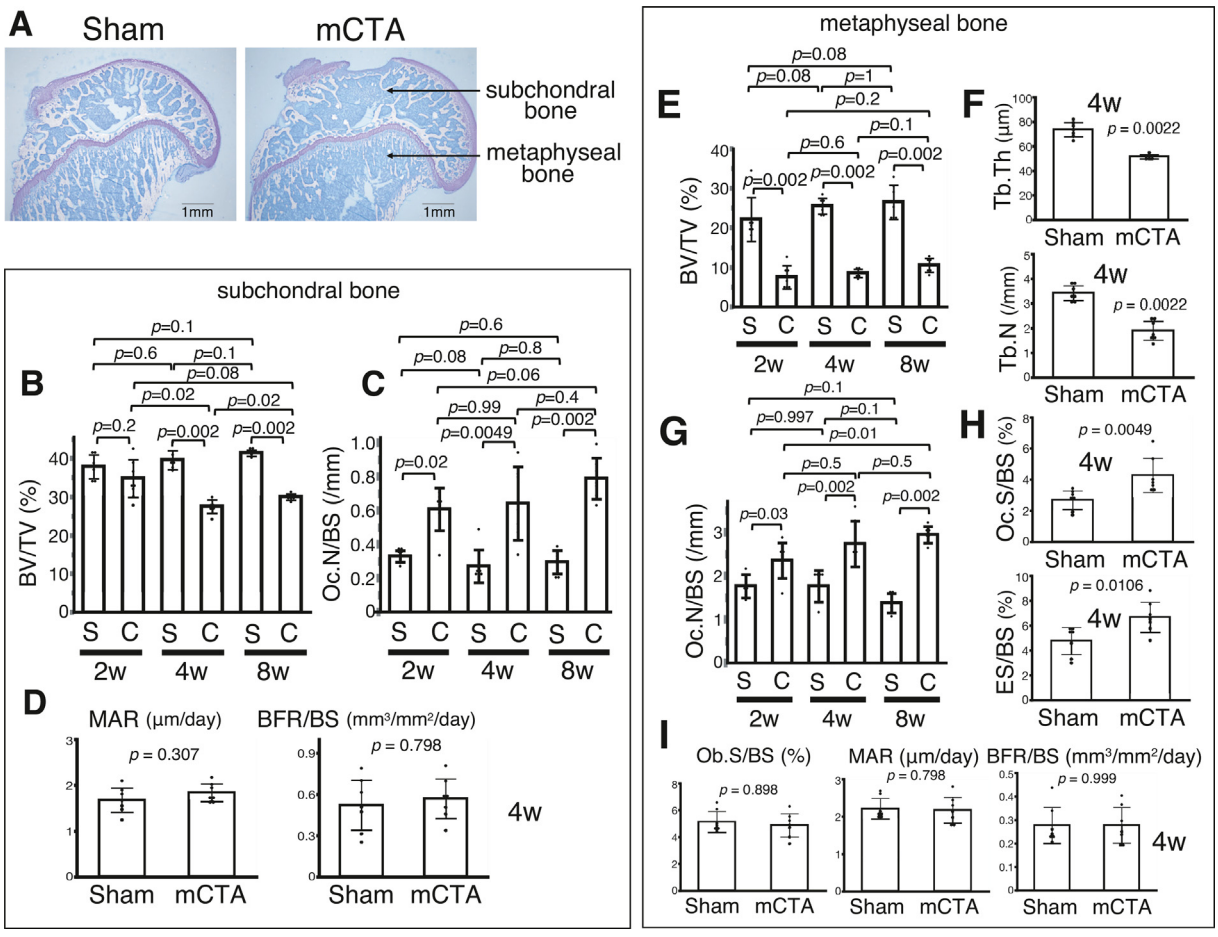

Fig. 6. Bone histomorphometry of mCTA-affected humeral head. (A) Toluidine blue staining of the undecalcified humeral head specimen was performed for bone histomorphometry. Subchondral bone and metaphyseal bone are indicated by arrows. (B–D) BV/TV, Oc.N/BS, MAR, and BFR/BS were examined in the subchondral bone area after indicated weeks of mCTA induction (n = 7). (E–I) BV/TV, Tb.Th, Tb.N, Oc.N/BS, Oc.S/BS, ES/BS, Ob.S/BS, MAR, and BFR/BS were examined in the metaphyseal bone area after indicated weeks of mCTA induction (n = 7). S = Sham; C = mCTA. The Wilcoxon rank-sum test was performed. mCTA, modified cuff tear arthropathy; BV/TV, bone volume fraction; Tb.Th, trabecular thickness; Tb.N, trabecular number; Oc.N/BS, number of osteoclasts per unit of bone surface; Oc.S/BS, osteoclast surface per unit of bone surface; ES/BS, eroded surface per unit of bone surface; Ob.S/BS, osteoblast surface per unit of bone surface; MAR, mineral apposition rate; BFR/BS, bone formation rate per unit of bone surface.

mCTA synovium. However, IL-6, MMP-3, and MMP-13 showed low expression levels (Fig. 5), suggesting that human OA and our rat mCTA model have slightly different pathophysiology.

In the early stage of OA, enhanced subchondral bone turnover is observed, and the subchondral bone plate becomes thinner and more porous until it is osteoporotic, implicating enhanced osteoclast-mediated bone resorption [36]. Conversely, in late-stage OA, the subchondral bone becomes thicker and sclerotic [36]. In human CTA cases, the spongiosa of the humeral head becomes osteoporotic [4]. Our rat model of mCTA showed an approximately 25% decrease in subchondral bone volume at 4

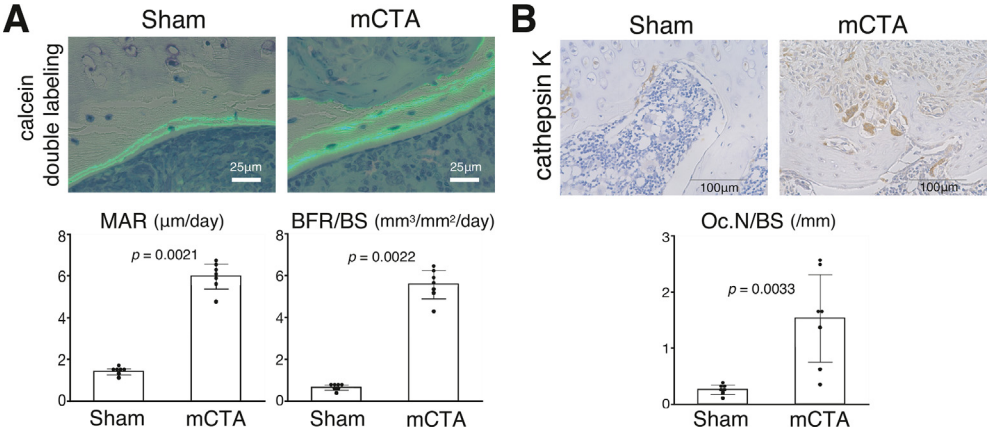

Fig. 7. Enhanced bone formation and resorption in collapsed subchondral bone of mCTA-affected humeri. (A) Upper panels: merged images of calcein fluorescence and toluidine blue staining in the collapsed subchondral bone area 4 weeks after mCTA induction. Lower panels: MAR and BFR/BS were examined (n = 7). (B) Upper panels: immunohistochemistry for cathepsin K was performed to detect osteoclasts in the collapsed subchondral bone area. Lower panel: Oc.N/BS was examined (n = 7). The Wilcoxon rank-sum test was performed. mCTA, modified cuff tear arthropathy; MAR, mineral apposition rate; BFR/BS, bone formation rate per unit of bone surface; Oc.N/BS, number of osteoclasts per unit of bone surface.

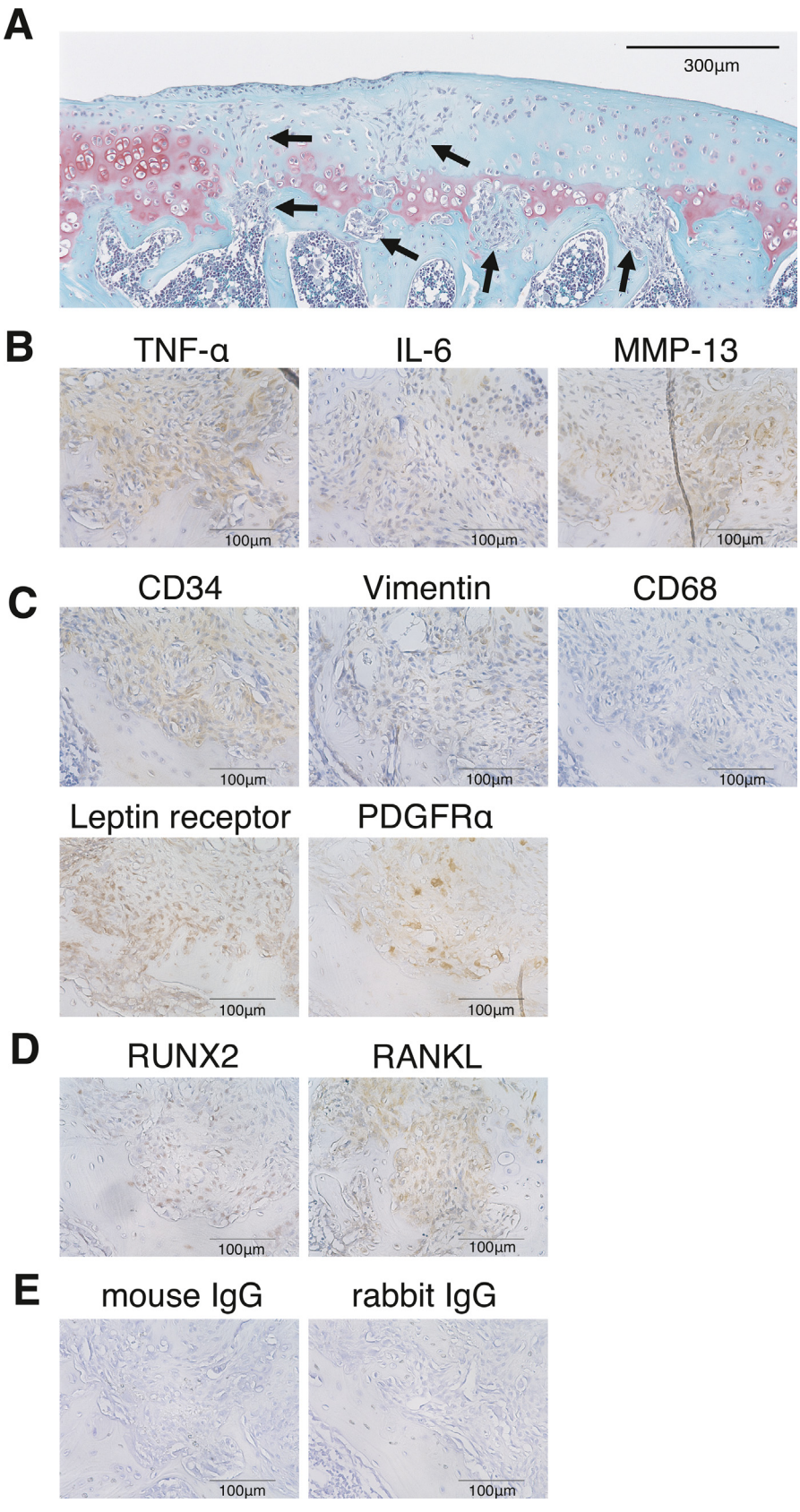

Fig. 8. Characterization of fibrous cells residing adjacent to collapsed subchondral bone in mCTA-affected humeral head. (A) Safranin O-stained image of superior cartilage area of the mCTA-affected humeral head 4 weeks after induction, demonstrating fibrous cells (arrows) invading the subchondral bone and cartilage that seem to have gained access from the bone marrow. (B–D) Immunohistochemistry of the indicated proteins on the fibrous cells residing adjacent to the collapsed subchondral bone in the mCTA humeral head. (E) Normal mouse IgG and normal rabbit IgG served as negative controls for the primary antibodies. mCTA, modified cuff tear arthropathy; TNF, tumor necrosis factor; IL, interleukin; MMP, matrix metalloproteinase; PDGFR, platelet-derived growth factor receptor.

weeks (accounting for 3 human life years) after induction (Fig. 6B), and this bone loss is comparable to the result at 29 weeks (accounting for 23 human life years) in the mouse model of RCT alone [10]. Unexpectedly, we found that the trabecular bone volume of the metaphyseal area was also remarkably reduced in the mCTA-affected humeri within 2 weeks (Fig. 6E). To the best of our knowledge, this is the first report to describe the bone loss in the metaphyseal spongiosa of CTA-affected humeri in either humans or animals. In both areas of the subchondral bone and metaphysis, osteoclasts were increased whereas bone formation parameters were unaffected, indicating uncoupling of osteoblast and osteoclast activities (Fig. 6).

Subchondral bone collapse in the superior part of the humeral head is the characteristic feature of CTA [4], and it was clearly reproduced in our rat mCTA model. At the beginning of this study, we had speculated that the subchondral bone collapse is a result of direct physical impacts between the humeral head and the acromion after the rotator cuff tears. However, in our mCTA model, it appears that the detached rotator cuff immediately undergoes scar healing, preventing superior migration of the humeral head (Fig. 3D), suggesting that the severe bone loss in the subchondral bone region is one of the causes of the collapse. Moreover, as mentioned in the introduction, the concept of the superior capsule as a hammock-like structure and the suspension bridge phenomenon [3] is crucial. Therefore, in addition to high resorption-induced and possibly disuse-induced bone atrophy in mCTA-affected humeri, damage to these structures may potentially contribute to biomechanical stress on the humeral head, leading to the collapse.

Another characteristic feature of CTA is the fibrous cells covering the humeral head cartilage. In OA cartilage, pannus-like fibrous cells express IL-1β, MMP-1, MMP-3, and MMP-13 [37,38], and these cells are speculated to be derived from bone marrow MSCs because they gain access to the joint surface through gaps in the subchondral bone plate, and these cells express vimentin and CD34 [39] but are negative for CD68 [38]. We immunohistochemically characterized the mCTA fibrous cells and found that the protein expression profile was similar to that of OA fibrous cells (Fig. 8). We additionally evaluated the expression of the specific MSC markers leptin receptor and PDGFRα, confirming their positive staining in the fibrous cells (Fig. 8C). This suggested that their origin was MSCs. Indeed, these cells seemed to gain access to the joint surface through gaps in the collapsed subchondral bone from the bone marrow (Fig. 8A). Although RA pannus cells express RANKL [40], this expression has not been reported in OA fibrous cells. In the present study, we found RANKL expression in the fibrous cells of the mCTA-affected humeral head (Fig. 8D). In the repair tissue of late-stage OA, multipotent stem cell-like cells called chondrogenic progenitor cells (CPCs) were identified [41]. These cells exhibit high migratory potential and are positive for MSC markers; can differentiate into osteoblasts and chondrocytes; and are under the control of osteoblastic RUNX2 and chondrocytic SOX9 [41]. Because RUNX2 induces RANKL expression in osteoblasts to promote osteoclastogenesis of bone marrow cells [42], the fibrous cells in our mCTA model may have gained the osteoblastic characteristics necessary to express RANKL for stimulating osteoclastogenesis [42,43]. Further studies are needed to investigate whether fibrous cells play a role in inducing osteoclast differentiation and promoting subchondral bone defects, potentially through the use of an mCTA model with fibrous cell-specific Cre (induced by an MSC marker) for inducible loss of RANKL. Depending on the results, anti-osteoclast drugs such as anti-RANKL antibody might be useful to prevent humeral head collapse in CTA cases.

This study had some limitations. First, because the extent of capsule damage in human CTA cases has not been evaluated, whether the resection range of the upper capsule in our mCTA model reflects the exact situation in human CTA remains unclear. The severity of the resulting arthropathy associated with various capsule resection ranges needs to be evaluated. Furthermore, it remains unclear whether the defects in the superior capsule, the rotator cuff and the LHB contribute independently to the changes observed in our model. Due to the proximity of the superior capsule to the rotator cuff, the surgical removal of only the capsule can present technical challenges, although it is worth considering the development of such a model in future research. Second, in our mCTA model, there were no changes detected by X-ray examination at 4 weeks after induction, and it did not progress to end-stage CTA with humeral head destruction equivalent to Hamada grade 5^{6} (Fig. 3F). There is a possibility that it may take more time for detectable changes in the humeral head of mCTA to occur on X-ray. However, even from Hamada grade 2 onwards, irregularities in the humeral head joint surface are observed [6]. The irregularities on X-rays may indicate local collapse, and it is possible that more collapses are occurring in clinical practice. Therefore, there is a discrepancy between X-rays and histopathological images in the detection of collapse, suggesting that histopathological examination has a higher sensitivity in detecting collapse. Third, although rats were found to be an appropriate *in vivo* animal model for studying rotator cuff disease [8], it is important to clarify that this suitability arises from their anatomical and morphological similarities to humans. However, functionally, as quadrupedal animals that primarily load weight on their forelimbs, they are not the optimal model. The anatomical and functional differences between shoulder joints in rats and humans might be the reason why we did not observe other specific features of CTA, such as femoralization or acetabularization [7]. In that case, primates like the cynomolgus monkey might be more suitable. Finally, because rats seem to have a high self-healing capacity to reconnect the resected rotator cuff tendon with scar tissue within 2 weeks (Fig. 3D) in spite of the increased instability by the combined transection of the LHB and the capsule, this is not a pure "cuff tear" arthropathy model; such spontaneous healing does not occur in the human shoulder. Indeed, research has shown that scar tissue formation and healing of rotator cuff injury occurs in rats [44].

In conclusion, compared to the sole rotator cuff resection, additional detachment of the LHB and the capsuloligamentous complex induced arthropathy, characterized by subchondral bone collapse within a reasonable timeframe. Fibrous cells accumulated around the subchondral bone collapse site, and expressed markers associated with OA, MSC markers and RANKL, although the specific role of these cells remains unclear and represents an area for future investigation.

Author contributions

Conception and design of the study: TIj, SM, NT. Acquisition of data: TIj, TIu, HT, YM. Analysis and interpretation of data: TIj, TIu, SM. Drafting of the article: TIj SM. Critical revision of the article: TIj, SM, NT. Statistical expertise: AT. Final approval of the article: TIj, TIu, HT, YM, AT, SM, NT. Acquisition of funding: SM, NT. TIj (iju.iju.1111@icloud.com), SM (s-maeda@m3.kufm.kagoshima-u.ac.jp) and NT (tanigu@m2.kufm.kagoshima-u.ac.jp) take responsibility for the integrity of the work as a whole, from inception to finished article.

Role of the funding source

This study was supported by the Japan Society for the Promotion of Science Grant-in-Aid for Scientific Research (C) (contract nos. 20K09482, 21K09303, 21K09253, 22K09336, and 22K09309). The funding source had no role in the study design; collection, analysis, or interpretation of data; writing of the manuscript; or decision to submit the manuscript.

Declaration of competing interest

For all authors, there are no conflict of interest to declare.

Acknowledgments

We are grateful to Hui Gao and Miki Sakoda for providing technical assistance. We also thank Angela Morben, DVM, ELS, from Edanz (https://jp.edanz.com/ac) for editing a draft of this manuscript.

Appendix A. Supplementary data

Supplementary data to this article can be found online at https://doi.org/10.1016/j.ocarto.2023.100389.

References

[1] M. Bahk, E. Keyurapan, A. Tasaki, E.L. Sauers, E.G. McFarland, Laxity testing of the shoulder: a review, Am. J. Sports Med. 35 (2007) 131–144.
[2] J.A. Abboud, L.J. Soslowsky, Interplay of the static and dynamic restraints in glenohumeral instability, Clin. Orthop. Relat. Res. (2002) 48–57.
[3] C.R. Adams, A.M. DeMartino, G. Rego, P.J. Denard, S.S. Burkhart, The rotatorcuff and the superior capsule: why we need both, Arthroscopy 32 (2016) 2628–2637.
[4] C.S. Neer 2nd, E.V. Craig, H. Fukuda, Cuff-tear arthropathy, J Bone Joint Surg Am 65 (1983) 1232–1244.
[5] M. Elsharkawi, B. Cakir, H. Reichel, T. Kappe, Reliability of radiologic glenohumeral osteoarthritis classifications, J. Shoulder Elbow Surg. 22 (2013) 1063–1067.
[6] K. Hamada, K. Yamanaka, Y. Uchiyama, T. Mikasa, M. Mikasa, A radiographic classification of massive rotator cuff tear arthritis, Clin. Orthop. Relat. Res. 469 (2011) 2452–2460.
[7] A. Eajazi, S. Kussman, C. LeBedis, A. Guermazi, A. Kompel, A. Jawa, et al., Rotator cuff tear arthropathy: pathophysiology, imaging characteristics, and treatment options, AJR Am. J. Roentgenol. 205 (2015) W502–W511.
[8] L.J. Soslowsky, J.E. Carpenter, C.M. DeBano, I. Banerji, M.R. Moalli, Development and use of an animal model for investigations on rotator cuff disease, J. Shoulder Elbow Surg. 5 (1996) 383–392.
[9] E.J. Kramer, B.M. Bodendorfer, D. Laron, J. Wong, H.T. Kim, X. Liu, et al., Evaluation of cartilage degeneration in a rat model of rotator cuff tear arthropathy, J. Shoulder Elbow Surg. 22 (2013) 1702–1709.
[10] A. Zingman, H. Li, L. Sundem, B. DeHority, M. Geary, T. Fussel, et al., Shoulder arthritis secondary to rotator cuff tear: a reproducible murine model and histopathologic scoring system, J. Orthop. Res. 35 (2017) 506–514.
[11] P.N. Chalmers, D.H. Salazar, K. Steger-May, A.M. Chamberlain, G. Stobbs-Cucchi, K. Yamaguchi, et al., Radiographic progression of arthritic changes in shoulders with degenerative rotator cuff tears, J. Shoulder Elbow Surg. 25 (2016) 1749–1755.
[12] R. Furuhata, N. Matsumura, S. Oki, T. Nishikawa, H. Kimura, T. Suzuki, et al., Risk factors of radiographic severity of massive rotator cuff tear, Sci. Rep. 12 (2022) 13567.
[13] S. Dutta, P. Sengupta, Men and mice: relating their ages, Life Sci. 152 (2016) 244–248.
[14] P. Sengupta, The laboratory rat: relating its Age with Human's, Int. J. Prev. Med. 4 (2013) 624–630.
[15] K. Kikukawa, J. Ide, K. Kikuchi, M. Morita, H. Mizuta, H. Ogata, Hypertrophic changes of the teres minor muscle in rotator cuff tears: quantitative evaluation by magnetic resonance imaging, J. Shoulder Elbow Surg. 23 (2014) 1800–1805.
[16] J. Steinbeck, U. Liljenqvist, J. Jerosch, The anatomy of the glenohumeral ligamentous complex and its contribution to anterior shoulder stability, J. Shoulder Elbow Surg. 7 (1998) 122–126.
[17] Y. Itoigawa, E. Itoi, Y. Sakoma, N. Yamamoto, H. Sano, K. Kaneko, Attachment of the anteroinferior glenohumeral ligament-labrum complex to the glenoid: an anatomic study, Arthroscopy 28 (2012) 1628–1633.
[18] Z. Czyrny, B. Kordasiewicz, M. Kicinski, M. Brzozowska, Macroscopic and ultrasonographic anatomy of the rotator cuff layers, J Ultrason 19 (2019) 120–124.
[19] T. Mihata, T.Q. Lee, C. Watanabe, K. Fukunishi, M. Ohue, T. Tsujimura, et al., Clinical results of arthroscopic superior capsule reconstruction for irreparable rotator cuff tears, Arthroscopy 29 (2013) 459–470.
[20] E. Itoi, D.K. Kuechle, S.R. Newman, B.F. Morrey, K.N. An, Stabilising function of the biceps in stable and unstable shoulders, J Bone Joint Surg Br 75 (1993) 546–550.
[21] T. Youm, N.S. ElAttrache, J.E. Tibone, M.H. McGarry, T.Q. Lee, The effect of the long head of the biceps on glenohumeral kinematics, J. Shoulder Elbow Surg. 18 (2009) 122–129.
[22] G. Walch, T.B. Edwards, A. Boulahia, L. Nove-Josserand, L. Neyton, I. Szabo, Arthroscopic tenotomy of the long head of the biceps in the treatment of rotator cuff tears: clinical and radiographic results of 307 cases, J. Shoulder Elbow Surg. 14 (2005) 238–246.
[23] A. Hasegawa, T. Mihata, K. Fukunishi, A. Uchida, M. Neo, Relationship between the Hamada Grade and underlying pathological conditions in the rotator cuff and long head of biceps in symptomatic patients with rotator cuff tears, JSES Int 6 (2022) 488–494.
[24] B.O. Zhou, R. Yue, M.M. Murphy, J.G. Peyer, S.J. Morrison, Leptin-receptor-expressing mesenchymal stromal cells represent the main source of bone formed by adult bone marrow, Cell Stem Cell 15 (2014) 154–168.
[25] S. Morikawa, Y. Mabuchi, Y. Kubota, Y. Nagai, K. Niibe, E. Hiratsu, et al., Prospective identification, isolation, and systemic transplantation of multipotent mesenchymal stem cells in murine bone marrow, J. Exp. Med. 206 (2009) 2483–2496.
[26] T. Komori, H. Yagi, S. Nomura, A. Yamaguchi, K. Sasaki, K. Deguchi, et al., Targeted disruption of Cbfa1 results in a complete lack of bone formation owing to maturational arrest of osteoblasts, Cell 89 (1997) 755–764.
[27] K.E. Reuther, J.J. Sarver, S.M. Schultz, C.S. Lee, C.M. Sehgal, D.L. Glaser, et al., Glenoid cartilage mechanical properties decrease after rotator cuff tears in a rat model, J. Orthop. Res. 30 (2012) 1435–1439.
[28] T. Toma, N. Suenaga, N. Taniguchi, N. Oizumi, H. Yamaguchi, Y. Tome, et al., Humeral head histopathological changes in cuff tear arthropathy, J. Orthop. Surg. 27 (2019) 2309499018816428.
[29] M. Kapoor, J. Martel-Pelletier, D. Lajeunesse, J.P. Pelletier, H. Fahmi, Role of proinflammatory cytokines in the pathophysiology of osteoarthritis, Nat. Rev. Rheumatol. 7 (2011) 33–42.
[30] K.H. Kim, J.H. Jo, H.J. Cho, T.S. Park, T.M. Kim, Therapeutic potential of stem cell-derived extracellular vesicles in osteoarthritis: preclinical study findings, Lab Anim Res 36 (2020) 10.
[31] P. Reboul, J.P. Pelletier, G. Tardif, J.M. Cloutier, J. Martel-Pelletier, The new collagenase, collagenase-3, is expressed and synthesized by human chondrocytes but not by synoviocytes. A role in osteoarthritis, J. Clin. Invest. 97 (1996) 2011–2019.
[32] T. Funck-Brentano, M. Cohen-Solal, Crosstalk between cartilage and bone: when bone cytokines matter, Cytokine Growth Factor Rev. 22 (2011) 91–97.
[33] A. Latourte, C. Cherifi, J. Maillet, H.K. Ea, W. Bouaziz, T. Funck-Brentano, et al., Systemic inhibition of IL-6/Stat3 signalling protects against experimental osteoarthritis, Ann. Rheum. Dis. 76 (2017) 748–755.
[34] B.J. de Lange-Brokaar, A. Ioan-Facsinay, G.J. van Osch, A.M. Zuurmond, J. Schoones, R.E. Toes, et al., Synovial inflammation, immune cells and their cytokines in osteoarthritis: a review, Osteoarthritis Cartilage 20 (2012) 1484–1499.
[35] R.K. Davidson, J.G. Waters, L. Kevorkian, C. Darrah, A. Cooper, S.T. Donell, et al., Expression profiling of metalloproteinases and their inhibitors in synovium and cartilage, Arthritis Res. Ther. 8 (2006) R124.
[36] T. Hugle, J. Geurts, What drives osteoarthritis?-synovial versus subchondral bone pathology, Rheumatology 56 (2017) 1461–1471.
[37] G.H. Yuan, M. Tanaka, K. Masuko-Hongo, A. Shibakawa, T. Kato, K. Nishioka, et al., Characterization of cells from pannus-like tissue over articular cartilage of advanced osteoarthritis, Osteoarthritis Cartilage 12 (2004) 38–45.
[38] A. Shibakawa, H. Aoki, K. Masuko-Hongo, T. Kato, M. Tanaka, K. Nishioka, et al., Presence of pannus-like tissue on osteoarthritic cartilage and its histological character, Osteoarthritis Cartilage 11 (2003) 133–140.
[39] P.A. Duc, K. Yudoh, K. Masuko, T. Kato, K. Nishioka, H. Nakamura, Development and characteristics of pannus-like soft tissue in osteoarthritic articular surface in rat osteoarthritis model, Clin. Exp. Rheumatol. 26 (2008) 589–595.
[40] A.R. Pettit, N.C. Walsh, C. Manning, S.R. Goldring, E.M. Gravallese, RANKL protein is expressed at the pannus-bone interface at sites of articular bone erosion in rheumatoid arthritis, Rheumatology 45 (2006) 1068–1076.
[41] S. Koelling, J. Kruegel, M. Irmer, J.R. Path, B. Sadowski, X. Miro, et al., Migratory chondrogenic progenitor cells from repair tissue during the later stages of human osteoarthritis, Cell Stem Cell 4 (2009) 324–335.
[42] H. Enomoto, S. Shiojiri, K. Hoshi, T. Furuichi, R. Fukuyama, C.A. Yoshida, et al., Induction of osteoclast differentiation by Runx2 through receptor activator of nuclear factor-kappa B ligand (RANKL) and osteoprotegerin regulation and partial rescue of osteoclastogenesis in Runx2-/- mice by RANKL transgene, J. Biol. Chem. 278 (2003) 23971–23977.
[43] H. Yasuda, N. Shima, N. Nakagawa, K. Yamaguchi, M. Kinosaki, S. Mochizuki, et al., Osteoclast differentiation factor is a ligand for osteoprotegerin/osteoclastogenesis-inhibitory factor and is identical to TRANCE/RANKL, Proc. Natl. Acad. Sci. U. S. A. 95 (1998) 3597–3602.
[44] K.A. Derwin, A.R. Baker, J.P. Iannotti, J.A. McCarron, Preclinical models for translating regenerative medicine therapies for rotator cuff repair, Tissue Eng. B Rev. 16 (2010) 21–30.